

## H $\alpha$ measurements using DEFPOS/RTT150 Telescope: Instrumentation and observations

Muhittin Şahan<sup>1</sup>, İlhami Yeğingil<sup>2</sup> \* and Nazim Aksaker<sup>3</sup>

<sup>1</sup> Department of Technical Programs, Vocational School of Osmaniye, University of Osmaniye Korkut Ata, 80000, Osmaniye, Turkey; [msahan2000@yahoo.com](mailto:msahan2000@yahoo.com)

<sup>2</sup> Sultan Qaboos University, Department of Physics, College of Science, 123, Al-Khodh Muscat, Oman

<sup>3</sup> Department of Physics, Çukurova University, 01330, Adana, Turkey

Received 2008 June 27; accepted 2008 September 6

**Abstract** To investigate the physical properties of HII regions and some PNe about 4' in size, a DEFPOS Fabry-Perot spectrometer has been redesigned and set up at the coudé exit of the 150 cm RTT150 telescope (f/48) at TUBITAK National Observatory (Antalya/Bakırlitepe, Turkey). The spectrometer has a 4' circular field of view and a velocity resolution of 27.27 km s<sup>-1</sup> (a spectral resolving power of 11 000) over a 200 km s<sup>-1</sup> spectral window near H $\alpha$ . This work presents the details of the newly redesigned instrument for coudé observations, the data reduction techniques and finally presents some physical results of our new H $\alpha$  observations selected from the Reynolds et al. (2005) and Fich et al. (1990) papers. The DEFPOS system has been fully tested and the first observations of HII regions and PNe in the Galaxy are used to illustrate the power of the instrument. We feel that our first Fabry-Perot observations can provide a powerful tool for the study of objects with small angular size. In the future, we are planning to prepare a catalog including some physical properties such as radial velocity, line width, and intensity of some PNe and HII regions close to the 4' field of view.

**Key words:** instrumentation: adaptive optics, interferometers — methods: data analysis — ISM: HII regions, planetary nebulae: general — techniques: spectroscopic, radial velocities

### 1 INTRODUCTION

Warm Ionized Medium (WIM: also referred as the Diffuse Ionized Gas: DIG or Reynolds layers) is known as a major component of the interstellar medium (hereafter referred to as ISM) and consists of warm temperature ( $\approx 10^4$  K), low-density ( $\approx 0.1$  cm<sup>-3</sup>) ionized hydrogen regions that occupy approximately 20% of the volume within a 2 kpc (1 pc =  $3.086 \times 10^{13}$  km) thick layer about the Galactic midplane (Tufté 1997; Haffner et al. 1999; Ferrière 2001; Reynolds 2004). Although originally detected in the 1960s with radio techniques (Hoyle & Ellis 1963), developments in Fabry-Perot spectrometers have shown that the primary source of information about the physical properties of the WIM has been obtained through the detection and study of faint, diffuse interstellar emission lines at optical wavelengths (Reynolds 1991; Tufté 1997; Haffner et al. 1998, 2003; Reynolds 2004). Since Fabry-Perot spectrometers have high throughput (or luminosity) and high spectral resolution, they are particularly well suited for detailed studies of diffuse the H $\alpha$  emission lines (Roesler 1974; Nossal et al. 2001;

---

\* On leave of absence from Çukurova University

Şahan et al. 2007). The warm ionized hydrogen has therefore been observed in nearly all directions of the Milky Way Galaxy with these emission lines. Much progress has been made in revolutionizing our understanding of the distribution and kinematics of the WIM.

Reynolds et al. (1973, 1974) have firstly measured faint optical emission lines with a Fabry-Perot spectrometer at the coudé focus of Goddard Space Flight Center's 91-cm telescope in Greenbelt, Maryland. In succeeding years, many  $H\alpha$  emission line measurements from the ISM and geocorona have been made regularly by a group of researchers from the University of Wisconsin (Roesler 1974; Reynolds 1988; Reynolds et al. 1990; Shih et al. 1985; Nossal et al. 1997; Mierkiewicz 2002) and many physical and kinematical properties of the HII regions (e.g., intensity, radial velocity, and temperature) have been determined in these studies. At the beginning of the 1990s, the development of the Charged Coupled Device (CCD) camera technology enabled an increase in the sensitivity of Fabry-Perot observations of faint sources in the ISM (Reynolds et al. 1990; Nossal et al. 2004). Because of high quantum efficiency, CCD cameras collect light simultaneously in multiple spectral bins and provide a 10 to 20 fold saving in integration time (Nossal et al. 1998).

The Wisconsin group is currently operating two Fabry-Perot spectrometers for emission line studies. One instrument is WHAM (Wisconsin Hydrogen Alpha Mapper) which is a Fabry-Perot spectrometer located at Kitt Peak National Observatory, Arizona (Haffner et al. 2003). The WHAM consists of a 15 cm aperture, dual etalon Fabry-Perot spectrometer coupled to a 0.6 m aperture siderostat, which provides a one degree diameter beam on the sky (Tufté 1997). The recently completed the WHAM Northern Sky  $H\alpha$  Survey (WHAM NSS), including more than 37 000 spectra, has provided the first map of the large scale distribution and kinematics of the diffuse ionized gas in the Galaxy above the declination  $-30^\circ$  (Haffner et al. 2003; Reynolds 2004). The second instrument is a 15 cm large aperture, double-etalon Fabry-Perot spectrometer located west of Madison at Pine Bluff Observatory (PBO). The PBO spectrometer was designed to investigate the influence of the solar cycle variation on the Earth's upper atmosphere with geocoronal  $H\alpha$  emission lines. This facility has an optical field of view (hereafter FOV) of  $1.5^\circ$  of the sky, and a spectral range of  $75 \text{ km s}^{-1}$  at  $H\alpha$  with  $3.75 \text{ km s}^{-1}$  spectral resolution (Mierkiewicz et al. 2006; Nossal et al. 2006).

Similar to the WHAM instrument, in 2002, a Dual Etalon Fabry-Perot Optical Spectrometer (DEFPOS) was designed to be used at the coudé exit of the 150 cm telescope at TUBITAK National Observatory (TUG) at Bakırlitepe ( $36^\circ 51'N$ ;  $30^\circ 20'E$ ; elevation: 2547 m, Antalya/Turkey) (Şahan et al. 2005, 2007). However, since the coudé exit of the telescope was not ready for spectroscopic observations until 2005, the spectrometer was previously operated in the zenith direction with a large angular resolution of  $4.76^\circ$  for two years (2002 November – 2004 December). Galactic (Şahan et al. 2005) and geocoronal  $H\alpha$  lines (Şahan et al. 2007) were measured during these observations. After completing test observations in the zenith direction, the spectrometer has been newly redesigned for coudé observations in 2007 and then set up at the coudé exit of the telescope to detect and study the faint optical emission lines from selected HII regions and Planetary Nebulae (hereafter PNe) with small angular sizes near the  $4'$  FOV. Additional earlier information about DEFPOS for zenith observations can be found in Şahan et al. (2005, 2007). This paper is organized as follows: Section 2 presents details about the optical design of the DEFPOS spectrometer. Intensity calibration is given in Section 3. Data reduction and data analysis of the Fabry-Perot spectrometer is given in Section 4. Discussion of our new  $H\alpha$  observations is given in Section 5, and finally conclusions are given in Section 6.

## 2 OBSERVATIONS

Since the Fabry-Perot Spectrometers offer sensitivities on the order of 100 to 300 times those of slits with dispersing elements of similar size, they are used to obtain high-resolution spectra of very faint, extended diffuse emission line objects of the ISM (Roesler 1974; Treffers 1981; Tufté 1997; Mierkiewicz 2002; Şahan et al. 2005). Details of the theory and application of the Fabry-Perot spectrometers were discussed by Roesler (1974), and Miller & Roesler (1998). In order to measure  $H\alpha$  emission lines from HII regions and PNe, about  $4'$  in size, the DEFPOS spectrometer is newly redesigned to be used at the coudé exit of the 150 cm telescope. Two main parts of the optical system are the RTT150 telescope and the

DEFPOS Fabry-Perot spectrometer. We will give details of the new optical design of the spectrometer after describing the basic properties of the telescope's optics.

## 2.1 RTT150 Telescope

TUBITAK National Observatory (TUG, established on Mount Bakırlitepe, Antalya/Turkey) has a 150 cm telescope, which is a Russian-Turkish Joint Telescope called RTT150. The RTT150 has two Cassegrain foci at  $f/8$  and  $f/16$ , and one coudé focus at  $f/48$  (Aslan 2003). For coudé observations, six mirrors at different points are used in the telescope system (Fig. 1). Light from the sky is reflected by the primary main mirror M1 ( $d = 150$  cm) to the secondary mirror M2, which sends the converging beam of light to the system of four flat mirrors M3, M4, M5 and M6, respectively. That allows the beam of light to leave the telescope strictly along its polar axis and to be collected in the coudé focus. Light then enters the coudé room. The focal length of the primary mirror (M1) is 7225.7 cm ( $f/48$ ) and the telescope has a  $3' 50''$  ( $\approx 4' \approx 0.064^\circ$ ) FOV when used for coudé observations. Detailed information about the RTT150 can be found in <http://www.tug.tubitak.gov.tr/>.

## 2.2 DEFPOS Spectrometer

The DEFPOS spectrometer is especially designed to obtain H $\alpha$  emission lines from extended diffuse emission lines from HII regions and PNe and utilizes a CCD as a detector. A simplified schematic diagram of the spectrometer located at the coudé room is shown in Figure 1. Figure 1 presents a combination of spectrometer and telescope optics. The spectrometer consists of pre-etalon (or entrance) optics, Fabry-Perot etalons (hereafter noted FP), post-etalon (or exit) optics, and finally a CCD imaging camera from top to bottom, respectively. These components are described in more detail in the following steps. Light from a chosen direction in the sky with  $4'$  FOV enters the telescope. After reflecting through the six mirrors, the light enters the coudé room and passes through two lenses and then is guided by a folding mirror (located just above the filter and not shown here) into the spectrometer that sends it down through the IF filter, and through the two FP etalons chambers, and finally passes through the camera lens onto the CCD chip.

### 2.2.1 Pre-Etalon optics

In order to achieve a maximum spectral resolution, light from the telescope must pass through the etalons. The total solid angle ( $\Omega$ ) of the light passing through the etalon is related to the maximum velocity resolution,  $\Omega/2\pi = \delta v/c$ , where  $\delta v$  and  $c$  is spectral resolution and velocity of light in units of  $\text{km s}^{-1}$ , respectively. The product of the area ( $A$ ) and the solid angle is known as the throughput (or etendue), which is constant at any image or pupil in the optical system. This equation therefore gives the limit to the maximum throughput ( $A\Omega$ ) of the DEFPOS for a given velocity resolution and an etalon area. This limit also equals the product of the area aperture (150 cm) and the FOV ( $4'$ ) of the RTT150 (Roesler 1974). As mentioned in the previous section, if light from the telescope with a FOV of  $4'$  ( $0.064^\circ$ ) is directly imaged between the etalons, and if the full frame of the etalons (7.5 cm) are used, in this case, light from the RTT150 will be focused with a small angle of  $0.64^\circ$  (corresponding to  $18.7 \text{ km s}^{-1}$ ) according to the etendue conservation relationship. However, since the emission line from the WIM have widths of  $15\text{--}50 \text{ km s}^{-1}$  and the motion of the gas is usually within  $\pm 100 \text{ km s}^{-1}$  of the Local Standard of Rest (LSR) (Tufty 1997), we made a new design and used a two lens combination before the etalons to obtain  $2.09^\circ$  filling angles, which corresponds to  $200 \text{ km s}^{-1}$  ( $4.4 \text{ \AA}$ ) velocity interval (Reynolds, private communication). The first lens (L1:  $f/22$ ), with a focal length of 430 cm ( $d \geq 10$  cm), was located just after the coudé exit of the telescope behind the focal point of 500 cm. The position of L1 was set so as to first focus (SKY1) light from the telescope. The first SKY1 image of the sky is behind the focal point of 170 cm, and has a diameter of size 3.7 cm. In order to perform an important nebular calibration study, it is helpful to image the sky (SKY1) between FP etalons (Mierkiewicz 2002). Therefore, with this field and for a desired  $200 \text{ km s}^{-1}$  spectral range, conservation of etendue requires

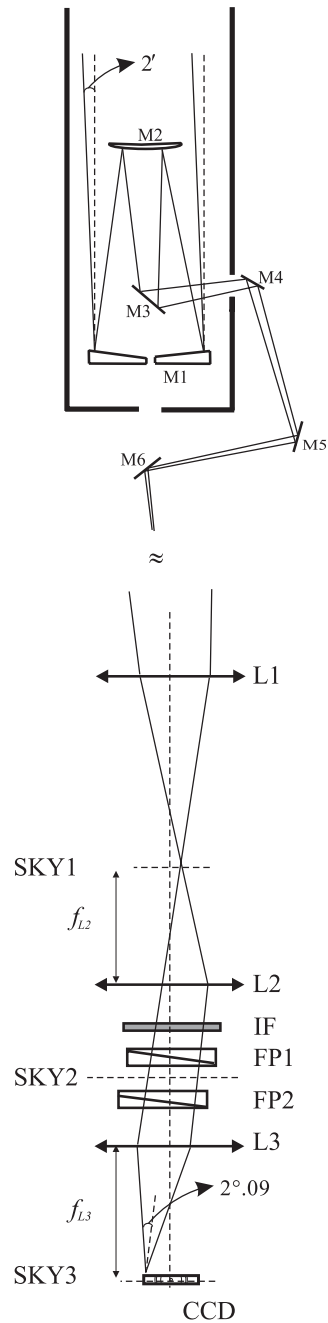


**Fig. 1** The basic optical diagram of the RTT150 Telescope and the DEFPOS Fabry-Perot spectrometer at the coudé focus of the telescope  $f/48$  (not to scale). Light from the sky is directed to the coudé exit by six mirrors of the telescope and enters the coudé room. Then, the light from the coudé exit of the telescope is firstly focused (SKY1) before the etalons by lens L1 ( $f_{L1}=430$  cm,  $f/22$ ). The second lens L2 ( $f_{L2}=50$  cm,  $d=6$  cm) located just above the IF filter produces a parallel beam passing through IF and then refocuses the SKY2 image between the etalons. Lens L3 ( $f_{\text{eff}}=f_{L3}=17$  cm,  $d=10$  cm) focuses the ring image (SKY2) onto a  $1.0$  cm<sup>2</sup> region (SKY3) of the CCD chip. The optical conjugates are indicated by the solid rays.

a second lens (L2), which has a diameter of 6 cm and a focal length of 50 cm. L2, installed in front of the interference filter (IF), produces a parallel beam from the ring pattern (SKY1). This parallel beam is passed through the IF filter and is then refocused between the FP1 and FP2 etalons as a new image (SKY2) for the second time. Note that the ring image of SKY1 is at the focal point of the L2 (the distance between L1 and L2 is 280 cm). SKY2 image has a diameter of 3.2 cm, that is, a small area of the etalons is used to obtain the  $200 \text{ km s}^{-1}$  spectral interval. With the L1 and L2 combination, the light from all positions in the sky is uniformly distributed across the  $200 \text{ km s}^{-1}$  spectral interval from a  $4'$  circular path of sky (Haffner et al. 1998). An extra mirror (not presented in Fig. 1) was located between L1 and L2 so that light from the RTT150 is folded into the spectrometer. Note that L1 and L2 are multi-layer AR coated for visible spectrum, BK7, plano convex single element lenses, custom made by ALTECHNA Co Ltd, Lithuania.

A 75 mm diameter broad band ( $15 \text{ \AA}$  FWHM at H $\alpha$ ) interference filter was used on top of the first FP1 etalon (Şahan et al. 2005, 2007) to suppress unwanted orders and to reduce parasitic light near the hydrogen Balmer- $\alpha$  wavelength (Haffner et al. 1999).

### 2.2.2 Fabry-Perot etalons

A dual etalon configuration was used, in which both low resolution (FP1) and high resolution (FP2) etalons were combined in series (refer to Fig. 1). Each etalon consists of two 7.5 cm diameter parallel mirrors held apart by three holders. The facing surfaces of each etalon are coated with dielectric multi-layers and have a reflectance of 92% at H $\alpha$ , which plays an important role in achieving the high performance of the Fabry-Perot. When compared to single etalon Fabry-Perot systems, the dual etalon design provides superior ghost and other rejections, extends the free spectral range, and suppresses the broad Lorentzian-like wings of the Airy functions (Roesler 1974; Haffner et al. 1999; Mierkiewicz 2002; Haffner et al. 2003; Reynolds et al. 2004). The first FP1 and the second FP2 etalon have a fixed plate spacing of  $l_1=0.0100 \text{ cm}$ , and  $l_2=0.0198 \text{ cm}$ , respectively. Each etalon is housed in separate gas tight chambers where tuning and imaging are done. The  $N_2$  gas is used inside etalon chambers and the gas pressure inside each chamber is independent of the other. An automatic pressure control system is used to maintain the tune of the two Fabry-Perot etalons and allows the  $200 \text{ km s}^{-1}$  spectral window to be set anywhere between 0.3 and 1.8 bar (blue to red line). Light passing through the etalon gives rise to an annular interference pattern at infinity and each interference pattern corresponds to a wavelength, decreasing from center to edge. By altering the gas pressure inside the chambers, the wavelength transmitted by the etalon at a given  $\theta$  can be selected according to equation of  $2n_g l \cos \theta = m\lambda$ , where  $n_g$  is the index of refraction of the gas between the etalon plates,  $l$  is the plate spacing,  $\theta$  is the angle of incidence,  $m$  is the order of interference, and  $\lambda$  is the transmitted wavelength (Reynolds et al. 1990; Mierkiewicz 2002; Mierkiewicz et al. 2006).

### 2.2.3 Post-Etalon optics

L3 lens, which immediately follows etalon chamber FP2, includes a combination of two lenses with the same properties, and has an effective focal length of 17 cm ( $f_{\text{eff}} = f_{L3} = 17 \text{ cm}$ ). This lens combination refocuses the ring image (SKY2) passing through the etalons onto a  $1.0 \text{ cm}^2$  region (SKY3) of the CCD chip. This ring spectrum on the CCD has an azimuthally symmetric pattern about the optical axis. Due to the nature of the Fabry-Perot's dispersion relation, the radial width of an annular resolution element decreases with increasing radius such that equal spectral intervals correspond to a set of equal areas on the detector (Reynolds et al. 1990, 1998; Tufte 1997).

### 2.2.4 CCD camera

The imaging CCD used in the DEFPOS/Telescope system is a Loral LICK3  $2\text{k} \times 2\text{k}$  back illuminated and AR coated camera. The CCD, which has  $2048 \times 2048$  pixels of 15 square microns and has a scale of  $0.35 \text{ arcsec pixel}^{-1}$ , which is connected to a control card in a Sun Ultra 1 computer via fiber-optic

communications cable. The CCD chip is cooled with liquid nitrogen ( $LN_2$ ) to a temperature of about  $-110^\circ\text{C}$  and can record many spectral elements simultaneously (Reynolds et al. 1990, 1998). The CCD has a high quantum efficiency (Q.E.) of  $\approx 78\%$  at hydrogen Balmer  $\alpha$ .

### 3 INTENSITY CALIBRATION

In astronomical data, the intensity calibration of the sky is very important in order to compare with the results of other studies. For intensity calibration, it is necessary to maintain long term source stability. Since PNe sources are diffuse and outside of the Earth's atmosphere and also fill the Fabry-Perot's FOV, they are suitable for Fabry-Perot calibration (Nossal et al. 1993). One example of these sources is NGC 7000 (the North American Nebula: NAN), known as a very large emission nebula in Cygnus. The absolute intensity of the emission from NGC 7000 was determined by Scherb (1981) using the planetary nebula NGC 7662 and some standard stars as reference objects. Scherb (1981) measured the intensity of the NGC 7000 to be  $850 \pm 50\text{R}$  for a  $49'$  FOV using a Fabry-Perot spectrometer. This measurement was confirmed by Nossal (1994) by using a blackbody source. Therefore, the value found by Scherb (1981) has been used in all  $1^\circ$  WHAM (Haffner et al. 2003) and  $0.8^\circ$  Wisconsin PBO data sets (Nossal 1994; Mierkiewicz et al. 2006) (past and present).

For the intensity calibration of the DEFPOS spectrometer, we also decided to use  $H\alpha$  emission selected within  $1^\circ$  WHAM FOV from the NGC 7000, which is approximately the same area as the  $49'$  FOV used by Scherb (1981). We obtained a considerable number of  $H\alpha$  spectra from nine different regions within this region at different exposure times (60 s to 1200 s). One region was especially selected with the same region whose intensity value was estimated to be 900 R over the  $4'$  FOV by Morgenthaler et al. (2001). Therefore, many  $H\alpha$  spectra were taken from this region at different exposures. Comparing these spectra with 900 R, we determined that  $1\text{ ADU km s}^{-1}$  corresponded to 2337.4 R for a 1200 s exposure time. Thus, the intensity values of the other eight individual regions were determined using this value (900 R). In order to compare intensity values from this region, the VTSS (Virginia Tech Spectral Survey)  $H\alpha$  imaging map and Ishida & Kawajiri's digitized map were used. From the digitized map, the average  $H\alpha$  surface brightness of  $49'$  was calculated and then the intensity value of the nebula for a  $4'$  region was estimated to be approximately 940 R, rather comparable to the value (900 R) estimated by Morgenthaler et al. (2001). Comparing with  $850 \pm 50\text{R}$  for a  $49'$  FOV, we found that our value of 1.58 was higher than that of Scherb's. In fact, Scherb (1981) mentioned that the  $H\alpha$  surface brightness for a selected region on the Ishida & Kawajiri map was about a factor of  $1.5 \pm 0.2$  brighter than that estimated for the same region by Reynolds et al. (1973). Therefore, we divided the data obtained from the digitized map by a factor of 1.58 for correction and then we compared them with earlier results obtained by Ishida & Kawajiri (1968), Scherb (1981), Morgenthaler et al. (2001) and Haffner et al. (2003). We saw that the calibration was in close agreement. As a result, we decided to use the  $H\alpha$  surface brightness of NGC 7000, which is 900 R for  $4'$  DEFPOS FOV and then all DEFPOS data in units of ADU were converted to R units. The details of the intensity calibration can be found in Aksaker et al. (in preparation).

### 4 DATA REDUCTION AND DATA ANALYSIS

The data reduction process for optical emission-line observations using the DEFPOS Fabry-Perot interferometer mounted on the 150 cm RTT150 Telescope is described in detail. Due to the nature of Fabry-Perot spectrometers, the  $H\alpha$  line from diffuse sources is formed as a ring pattern between etalons and this ring pattern is saved by a CCD camera, which can record many spectral elements simultaneously (Coakley et al. 1996; Nossal et al. 1998). Before analyzing the data, a series of data reduction procedures were required to convert a CCD image into a line profile (Şahan et al. 2005, 2007). This technique includes bias and reflection subtraction, filtering the hot pixels produced by cosmic rays greater than  $3\sigma$ , and finally dividing by the flat-field. Hydrogen (H) and hydrogen-deuterium (H-D) lamp emissions, dark images, and flat field exposures were used in the analysis of the  $H\alpha$  data.

A dark image is simply an image taken with the camera's shutter closed and is used to capture the effects of the CCD's heat and background electronic noise depending upon the temperature of the chip

and the length of the exposure. Dark images are taken before and after each image with an exposure of the same length of time as the sky exposure and then subtracted from the image. In addition to raw and dark images, flat field images are taken while pointing the telescope at a uniformly illuminated screen located in the telescope's dome. The purpose of the flat-field is to correct the image for pixel to pixel variations in sensitivity due to vignetting within the optical system of the spectrometer (Nossal 1994; Mierkiewicz 2002). 20 minute integration times are used for each flat field image. The dark counts are removed from each sky image and from the flat-field images and then the reduced sky images are divided by the flat field.

After the CCD reduction procedure, the reduced data are converted into one dimensional spectra using an annular summing technique, which involves imaging the Fabry-Perot's annular fringe pattern onto the CCD (Coakley et al. 1996; Haffner et al. 2003; Nossal et al. 2004). For the ring summing procedure, we defined a 50-pixel (area) annular window to obtain one dimensional spectra from the CCD image and we averaged the intensities in all of the CCD pixels whose centers fell within an annulus. In this way, the CCD images were converted into line profiles. Each annular window corresponds to a  $4 \text{ km s}^{-1}$  spectral window (+ symbols in Fig. 2b). For DEFPOS with an optical FOV of  $4'$  in the sky, each position within the  $4'$  beam is equally sampled by each spectral element of the  $4 \text{ km s}^{-1}$  ( $0.087 \text{ \AA}$ ) spectral resolution at H $\alpha$  of  $200 \text{ km s}^{-1}$  (Tufté 1997). The details of the annular summing technique are found in Coakley et al. (1996) and Nossal et al. (1997).

One sample of the DEFPOS data analysis is given in Figure 2. Figure 2a shows an H $\alpha$  map of the Orion nebula which was developed by SHASSA (the Southern H-Alpha Sky Survey Atlas), which is a Robotic Wide-Angle imaging survey of the Southern Sky ( $\delta = +15^\circ$  to  $-90^\circ$ ) at H $\alpha$  (Gaustad et al. 2001). Since the Orion Nebula (M42, NGC 1976) is one of the most interesting HII regions (Sh2-281) and is the nearest star forming region, we took an H $\alpha$  spectrum of the nebula, which is represented with a blue circle in Figure 2a. The blue circle indicates the location ( $\alpha = 05^{\text{h}}35^{\text{m}}14^{\text{s}}.5$ ,  $\delta = -05^\circ25'30''.0$ , equinox=2000.0) and size of the region observed by a  $4'$  diameter beam of DEFPOS. The three green circles also show the nearest  $1^\circ$  WHAM data taken for the WHAM NSS map. Figure 2b shows the raw CCD image output from the Orion nebula with DEFPOS. This "ring image" taken on 2007 November 26 represents an H $\alpha$  spectrum within the  $4'$  diameter circular beam and covers a  $200 \text{ km s}^{-1}$  ( $4.4 \text{ \AA}$ ) spectrum. In general, the exposure times for observations in our H $\alpha$  measurements were between 300 seconds and 1800 seconds. For this spectrum, a 600 second integration time was used. There are two reflections with intensities of 7% and 4.5% in the CCD image. We estimate that these features arise from reflections of the glass between the etalon chambers. To correct for these effects, the raw CCD image is subtracted from itself before the ring-summing procedure. Using the property of equal area annuli corresponding to equal spectral intervals, this CCD image was converted to one dimensional line profiles after the annular-summing procedure was employed (Fig. 2c). Since the H $\alpha$  spectra provide detailed information about physical conditions (e.g., the distribution and the kinematics) of the gas from the ISM (Reynolds 1991), it is important that the intensity of the spectra are determined accurately.

In Figure 2c, the amplitude was plotted against the velocity frame in units of  $\text{km s}^{-1}$ . The individual data points represent spectral elements in  $4 \text{ km s}^{-1}$  velocity intervals plotted against radial velocity with respect to the LSR. Since the spectrum was approximately similar to a Gaussian shape, all data were fitted with Gaussian line profiles by a fitting program after the subtraction of a linear baseline in order to find a position, a line width and a relative amplitude (Şahan et al. 2007). The solid curve drawn through the spectral elements represents the best fit Gaussian emission component. The fringe width of an H $\alpha$  spectrum is indicative of the spectral resolving power when the Fabry-Perot interferometer is used as a spectrometer and the position indicates the velocity of the spectrum with respect to the LSR (Mierkiewicz 2002). The horizontal axis was plotted according to the LSR velocity. The LSR velocity of the nebula is illustrated as a vertical dashed line at  $-11.36 \text{ km s}^{-1}$ . Velocity of the data from the Orion nebula is approximately  $0.01 \pm 0.3 \text{ km s}^{-1}$  with respect to the LSR velocity and the line width and the intensity of this spectrum are  $52.29 \pm 0.3 \text{ km s}^{-1}$  and  $121206.2 \pm 1597.7R$ , respectively. 1 Rayleigh (R) is  $10^6/4\pi \text{ photons cm}^{-2} \text{ sr}^{-1} \text{ s}^{-1} = 2.41 \times 10^{-7} \text{ erg cm}^{-2} \text{ s}^{-1} \text{ sr}^{-1}$  at H $\alpha$  and corresponds to an emission measure (EM =  $\int n_e^2 dl$ ) of  $2.3 \text{ cm}^{-6} \text{ pc}$  for a gas temperature of 8000 K, where  $n_e$  is the averaged electron density within an emitting region in the interstellar medium,  $dl$  is distance to this

region (Haffner et al. 2003; Reynolds et al. 2005). The residuals of the fit were plotted in the bottom panel in order to see the differences between the data and the fit.

## 5 DISCUSSION

The  $H\alpha$  emission line observations from HII regions provide a useful tool for the investigation of physical conditions of the ISM. The Fabry-Perot spectrometers are quite successful tools for studying diffuse ionized gas in the ISM. When Fabry-Perots are used in combination with a telescope and CCD, they have greater advantages than other kinds of spectrometers for studying diffuse regions. A 7.5 cm dual etalon DEFPOS Fabry-Perot spectrometer has been newly redesigned to be used at the coudé focus of the RTT150 telescope at TUG (TUBITAK National Observatory, Antalya/Turkey). The spectrometer has a resolving power of 11 000, corresponding to a velocity resolution of about  $30 \text{ km s}^{-1}$  (Şahan et al. 2005, 2007). The RTT150 telescope has a primary 150 cm ( $f/48$ ) mirror and has a  $4'$  FOV when used for coudé observations. The DEFPOS spectrometer therefore has a circular FOV of the sky of  $4'$  in diameter and a spectral range at hydrogen Balmer alpha of  $200 \text{ km s}^{-1}$  with a  $27.27 \text{ km s}^{-1}$  (FWHM) spectral resolution when used with the telescope. The spectrometer at the coudé exit enables a new look at the extremely narrow regions in the Galaxy compared with the  $1^\circ$  WHAM spectrometer (see Fig. 2a). Since the spectrometer has a narrow resolution of  $4'$  FOV and detects emissions from the small-sized regions in the ISM, longer integration times ranging from 300 to 1800 seconds were used to obtain reasonable signal to noise ratios. Galactic and geocoronal  $H\alpha$  lines are not able to be distinguished from each other at this resolution. However, the sources with small angular size ( $< 1^\circ$ ), which are not seen with  $1^\circ$  WHAM, will be examined in more detail by the DEFPOS. The absolute intensity calibration of the spectrometer was made by observing the center of NGC 7000. Below, we discuss the first observations obtained with DEFPOS at the coudé exit of the RTT150.

Since HII regions and the PNe are an important source for studying the ISM, it is important to understand the basic processes of these objects. Therefore,  $H\alpha$  observations of 100 objects with DEFPOS were carried out between 2007 May and 2007 November. The first data include a study of emission lines from HII regions and PNe with long exposure times. Due to the limited observation time available for the RTT150 telescope, it was possible to obtain a set of such data only for some spatial directions. Therefore, many of the data selected are from Reynolds et al.'s (2005) paper about PNe and from Fich et al.'s (1990) paper about HII regions. The goal of these observations was to test sensitivity of our spectrometer and to compare our results with other data from different spectrometers in the literature. Moreover, these data were also chosen because the line intensities were very bright sources which were necessary to obtain measurements in our available time. After we took the observations, the data reduction and ring summing were performed respectively as mentioned in the previous section. To determine the line widths (FWHM), the radial velocities with respect to the LSR, and the intensities of the data, Gaussian fits were applied to all of the data. Note that measuring the velocities of the HII regions or PNe is necessary for studying the distributions and motions of the ionized gas in the Galaxy.

Some sample data obtained from the first observations are given in Table 1. Table 1 includes some parameters for  $H\alpha$  emission components from the PNe regions, where the first column lists the names of PNe. The next two columns give the positions in 2000 coordinates. The succeeding fourth, fifth and sixth columns give intensity (R), the radial velocity (in  $\text{km s}^{-1}$ ) relative to the LSR and the line width (in  $\text{km s}^{-1}$ ), respectively. The final two columns give the reference values to be compared with DEFPOS data. We give a summary below of our first results given in Table 1.

NGC 3587 (Owl Nebula:  $\alpha=11^{\text{h}}14^{\text{m}}48^{\text{s}}.0$ ,  $\delta = 55^\circ 01' 00''.0$ , equinox=2000.0) is a planetary nebula with an angular diameter of  $3.4' \times 3.3'$ , and is about 0.8 kpc above the galactic midplane. It is important to observe this nebula with DEFPOS because it is small enough that the entire nebula can be measured with the  $4'$  FOV. Therefore, five  $H\alpha$  spectra from the nebula were taken on the nights of 2007 May 01/02 and May 02/03. The exposure times for observations ranged from 600 s to 1200 s. From observations of the nebula in a given night, mean LSR velocity and mean line-width of the NGC 3587 were measured to be  $+16.67 \text{ km s}^{-1}$  and to be  $70.53 \text{ km s}^{-1}$ , respectively. The mean intensity of the nebula was measured to be 498.5R. The LSR velocity and the mean line-width in the Reynolds et al. (2005) paper were 15

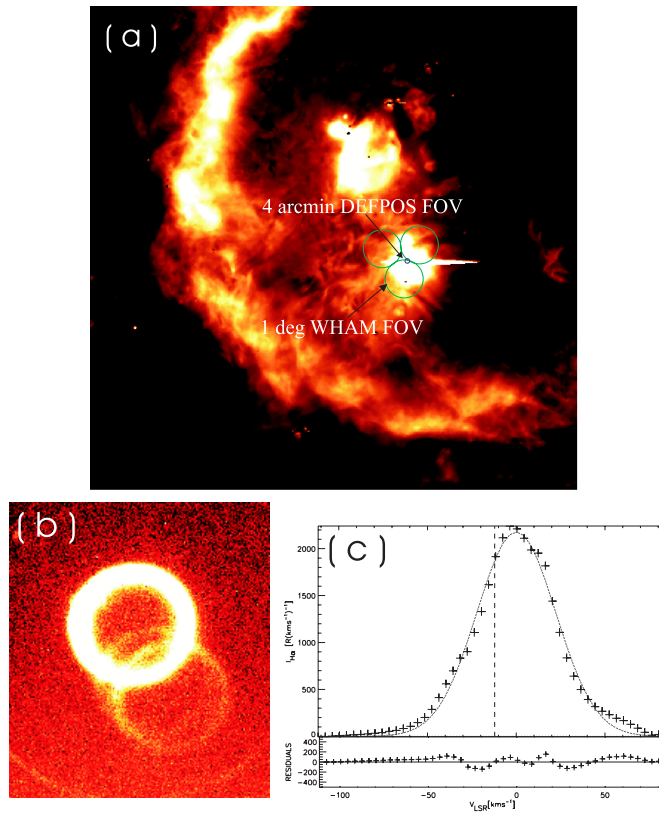


**Fig. 2** a) H $\alpha$  map of the Orion nebula developed by SHASSA (the Southern H-Alpha Sky Survey Atlas). The blue and green circles show the field of view of 4' DEFPOS and the field of view of 1 $^\circ$  WHAM, respectively. b) A raw CCD image from this blue point of the Orion Nebula within the 4' beam, on November 01, 2007. The exposure length for this image was 600 s. This image represents an H $\alpha$  spectrum within the 4' diameter circular beam and covers a 200 (4.4  $\text{\AA}$ ) spectrum. c) Line profile after the annular-summing procedure. The spectrum consists of 50 spectral elements corresponding to a 4 km s $^{-1}$  (0.087  $\text{\AA}$ ) spectral window (+ symbols). More detailed information about the figure can be found in the text.

$\pm 5$  km s $^{-1}$  and  $79 \pm 11$  km s $^{-1}$ , respectively. Schneider et al. (1983) also gave the LSR velocity of the nebula to be 11.5 km s $^{-1}$ .

The NGC 4361 planetary nebula (PNG 294+43:  $\alpha = 12^{\text{h}}24^{\text{m}}30^{\text{s}}.75$ ,  $\delta = -18^{\circ}47'05''.0$ , equinox=2000.0) has a high galactic latitude and has irregular structures in the surrounding shell (Chu et al. 1987; Muthu & Anandarao 2001). The nebula has an angular size of 1.8' at a distance of 0.7–1.9 kpc and was classified as a high-excitation planetary nebula. H $\alpha$  observations were made of the planetary nebula using DEFPOS on the night of 2007 November 25/26. The exposure time was 1800 s for this spectrum. The LSR velocity of the nebula was measured to be +15.45 km s $^{-1}$ . The line-width and the intensity of the nebula are 69.5 km s $^{-1}$  and 320.5 R, respectively. The radial velocity and the line width were found to be  $67 \pm 15$  km s $^{-1}$  and  $+12 \pm 7$  km s $^{-1}$ , respectively, by Reynolds et al. (2005). Moreover, the LSR velocity was also given to be +7.9 km s $^{-1}$  by Schneider et al. (1983).

NGC 6853, the Dumbbell Nebula (M27), is a planetary nebula in the constellation Vulpecula. NGC 6853, which has an angular diameter of  $8' \times 6'$ , was investigated using the H $\alpha$  line with a Fabry-Perot interferometer by Doroshenko (1998) in the past who measured the radial velocity to be  $-45 \pm 2$  km s $^{-1}$  relative to the sun and the mean half-width of the H $\alpha$  line to be  $41.5 \pm 4.5$  km s $^{-1}$ . Since

**Table 1** Some results of the DEFPOS/RTT150 system and references given in literature.

Sources	$\alpha$ 2000 (h m s)	$\delta$ 2000 ( $^{\circ}$ ' ")	$I_{H\alpha}$ (R*)	VLSR (km s $^{-1}$ )	FWHM (km s $^{-1}$ )	VLSR(ref) (km s $^{-1}$ )	FWHM (ref) (km s $^{-1}$ )
NGC 3587	11 14 48.0	55 01 00.0	498.5	+16.67	70.53	15 $\pm$ 5 <sup>a</sup> 11.5 <sup>b</sup>	79 $\pm$ 11 <sup>a</sup> –
NGC 4361	12 24 30.75	–18 47 05.0	320.5	+15.45	69.51	+12 $\pm$ 7 <sup>a</sup> +7.9 <sup>b</sup>	67 $\pm$ 15 <sup>a</sup> –
NGC 6853	19 59 36.34	+22 43 16.0	273.6	–42.80	34.00	–42 $\pm$ 5 <sup>c</sup> –45 $\pm$ 2 <sup>d</sup>	– 41.5 $\pm$ 4.5 <sup>d</sup>
NGC 7009	21 04 10.0	–11 21 48.0	235.3	–32.00	50.20	–40 $\pm$ 2 <sup>a</sup> –36.6 <sup>b</sup> –44 $\pm$ 3 <sup>e</sup> –53 $\pm$ 2 <sup>f</sup>	45 $\pm$ 1 <sup>a</sup> – – –
NGC 7293	22 29 38.0	–20 50 13.6	170.0	–29.4	43.60	–24 $\pm$ 1 <sup>a</sup> –25.0 <sup>b</sup>	40 $\pm$ 5 <sup>a</sup> –
NGC 7635	23 20 48.0	+61 12 06.0	745.2	–39.60	42.25	–	–
NGC 7662	23 25 53.0	+42 32 06.0	217.0	–7.20	49.60	–10 $\pm$ 1 <sup>a</sup> –12.2 $\pm$ 1 <sup>c</sup> –4.7 <sup>b</sup> –	49 $\pm$ 2 <sup>a</sup> – – 45 <sup>g</sup>

\*  $1 \text{ R} = 10^6/4\pi \text{ photons cm}^{-2}\text{sr}^{-1}\text{s}^{-1} = 2.41 \times 10^{-7} \text{ erg cm}^{-2} \text{ s}^{-1} \text{ sr}^{-1}$  at  $H\alpha$

<sup>a</sup> Reynolds et al. (2005)

<sup>b</sup> Schneider et al. (1983)

<sup>c</sup> Simbad Catalogue

<sup>d</sup> Doroshenko (1998)

<sup>e</sup> (the heliocentric velocity) Meatheringham et al. (1988)

<sup>f</sup> Fernández et al. (2004)

<sup>g</sup> Martin et al. (2004)

the diameter of the nebula fills DEFPOS' FOV, it is important for us to observe it. We have decided to undertake a more detailed study of NGC 6853 in order to understand its morphology. We thus made two observations in this direction ( $\alpha = 19^{\text{h}}59^{\text{m}}36^{\text{s}}.34$ ,  $\delta = +22^{\circ}43'16''.0$ , equinox=2000.0) on the night of 2007 May 01/02. The exposure length for this image was 1200 s. The radial velocity of the nebula was measured to be  $-42.80 \text{ km s}^{-1}$  relative to LSR. The mean line-width and the intensity of the nebula is  $34.00 \text{ km s}^{-1}$  and  $273.6 \text{ R}$ , respectively. The LSR velocity of the nebula is the same value given in the Simbad Catalog, which is approximately  $-42 \pm 5 \text{ km s}^{-1}$ . The value of DEFPOS agrees well with the determinations of other researchers.

NGC 7009 (PK 37–34 1, VG259, IRAS 21014–1133, Saturn Nebula:  $\alpha = 21^{\text{h}}04^{\text{m}}10^{\text{s}}.0$ ,  $\delta = -11^{\circ}21'48''.0$ , equinox=2000.0) is a bright planetary nebula with an angular diameter of  $60'' \times 40''$  at a distance of 0.73 kpc, located in the southern hemisphere in the constellation Aquarius. NGC 7009 was observed on 2007 November 25 with an exposure time of 1200 s. The LSR velocity of the nebula was measured to be  $-32.00 \text{ km s}^{-1}$ ; the line width and the surface brightness was measured to be  $50.20 \text{ km s}^{-1}$  and  $235.3 \text{ R}$ , respectively. Reynolds et al. (2005) also gave the radial velocity and line width of the nebula to be  $-40 \pm 2 \text{ km s}^{-1}$  and  $45 \pm 1 \text{ km s}^{-1}$ , respectively. Fernández et al. (2004) determined the radial velocity of the nebula to be  $-42 \pm 94 \text{ km s}^{-1}$  and a distance to be  $d = 0.86 \text{ kpc}$ . Meatheringham et al. (1988) measured the heliocentric velocity of the nebula to be  $-44 \pm 3 \text{ km s}^{-1}$ . Moreover, Schneider et al. (1983) measured the LSR velocity of the nebula to be  $-36.6 \text{ km s}^{-1}$ .

The planetary nebula NGC 7293 (the Helix nebula: PK 36–57 1,  $\alpha = 22^{\text{h}}29^{\text{m}}38^{\text{s}}.0$ ,  $\delta = -20^{\circ}50'13''.6$ , equinox=2000.0) discovered by Karl Ludwig Harding before 1824 is one of the closest nebulae to us with a distance of 0.15 kpc and an angular size of  $1.8'$  (Harris et al. 1997).  $H\alpha$  observations were made of the planetary nebula NGC 7293 on the night of 2007 November 25/26 with a 1200 s exposure length. The LSR velocity of the nebula was measured to be  $-29.4 \text{ km s}^{-1}$  and was also given to be  $-25.0 \text{ km s}^{-1}$  by Schneider et al. (1983). The line-width and the intensity of the nebula are

43.60 km s<sup>-1</sup> and 170.0 R, respectively. Reynolds et al. (2005) measured the velocity and the line width of the nebula to be  $-24 \pm 1$  km s<sup>-1</sup> and  $40 \pm 5$  km s<sup>-1</sup>, respectively.

The NGC 7635 nebula lying within the Perseus arm of the Galaxy is an emission region associated with an O6.5 IIIf located at  $\alpha = 23^{\text{h}}20^{\text{m}}48^{\text{s}}.0$ ,  $\delta = +61^{\circ}12'06''.0$ , equinox=2000.0 in the Cas OB2 association at a distance of 2.6 kpc (Humphreys 1978). The nebula is characterized by a striking emission ring with a radius of nearly  $1.66'$ , which gives the nebula its name: the Bubble nebula. The Bubble Nebula has an angular diameter of  $15.0' \times 8.0'$  and lies near a dark molecular cloud. The H $\alpha$  line spectrum was measured from the center of NGC 7635 with an exposure of 1200 s. The LSR velocity for the nebula was measured to be  $-39.60$  km s<sup>-1</sup>. The mean line-width and the intensity of the nebula were also measured to be  $42.25$  km s<sup>-1</sup> and 745.2 R, respectively.

NGC 7662 (Blue Snowball:  $\alpha = 23^{\text{h}}25^{\text{m}}53^{\text{s}}.0$ ,  $\delta = +42^{\circ}32'06''.0$ , equinox=2000.0) in the west of the constellation Andromeda has a bright main nebula that shows elliptical, double-shelled morphology. The high surface brightness makes it ideal for a detailed case study of the physical structure of elliptical PNe (Martin et al. 2004). The NGC 7662 has an angular size of  $20'' \times 14''$  (Guerrero et al. 1998) and the distance to this nebula was found by several authors including Daub (1982) (1.15 kpc) and Arsen & Terzian (1996) (0.79 kpc). The observations using the Fabry-Perot spectrometer of the nebula NGC 7662 were made on the night of 2007 May 02/03. The exposure times were 300 s and 1200 s. The radial velocity of NGC 7662 was measured to be  $-7.20$  km s<sup>-1</sup> relative to LSR. In the literature, the radial velocity of the nebula is given to be  $-12.2 \pm 1$  km s<sup>-1</sup> in the Simbad Catalog and to be  $-10 \pm 1$  km s<sup>-1</sup> in the paper of Reynolds et al. (2005). Moreover, the LSR velocity of the nebula was given to be  $-4.7$  km s<sup>-1</sup> by Schneider et al. (1983). The mean line-width and the intensity of the nebula are  $49.60 \pm 2.3$  km s<sup>-1</sup> and 217.0 R, respectively. The mean line width is given to be  $49 \pm 2$  km s<sup>-1</sup> by Reynolds et al. (2005), and to be  $+45$  km s<sup>-1</sup> by Martin et al. (2004). The results of the line width and the LSR velocity obtained with DEFPOS are thus consistent with the values given in the literature. By comparing these results obtained by the DEFPOS with the others reported in the literature for this object, the line width and the LSR velocity are approximately consistent.

## 6 CONCLUSIONS

Due to the extended nature of diffuse ionized gas, large aperture Fabry-Perot detection techniques have proven to be quite successful in studying the WIM. To determine some physical properties of the diffused ionized gas from some HII regions and PNe with small angular diameters, a 7.5 cm dual etalon DEFPOS Fabry-Perot spectrometer has been newly redesigned and attached to the  $f/48$  coudé focus of the RTT150 telescope at TUG (Antalya, Turkey). The spectrometer enables a new look at the extremely small angular size of PNe and HII regions in the Galaxy. After completing test studies in the coudé room, the first test observations were carried out with the DEFPOS/RTT150 system in 2007. We have compared our first observations and those from other studies of observed PNe in the literature to illustrate the power of the instrument. In conclusion, we think that our newly redesigned spectrometer can provide a powerful tool for the study of small angular-sized objects. In the future, we will prepare a catalog which includes some physical properties such as the radial velocity, the line width, and the intensity of HII regions and some PNe using the  $4'$  field of view.

**Acknowledgements** The authors would like to thank the TUG staff for help during the observations. The authors also wish to thank R. J. Reynolds, and L. M. Haffner, from the University of Wisconsin for letting us use their data and for having greatly contributed to the start of this study. We acknowledge the use of the VTSS map, a wide-field image survey of the Galaxy's warm ionized interstellar medium, the use of the SIMBAD Astronomical Database, operated at CDS, Strasbourg, France and the use of the Southern H-Alpha Sky Survey Atlas (SHASSA), which is supported by the National Science Foundation. This work is supported by TUBITAK (the Scientific and Technical Research Council of Turkey) with grant number 104T252.

## References

- Arsen, R. H., & Terzian, Y. 1996, *PASP*, 108, 419
- Aslan, Z. 2003, *The Magnetized Interstellar Medium*, Uyaniker, B., Reich, W., Wielebinski, R., eds, Copernicus GmbH, Katlenburg-Lindau, 215
- Chu, Y. H., Jacoby, G. H., & Arent, R. 1987, *ApJS*, 64, 529
- Coakley, M. M., Roesler, F. L., Reynolds, R. J., & Nossal, S. M. 1996, *Appl. Opt.*, 35, 6479
- Daub, C. T. 1982, *ApJ*, 260, 612
- Doroshenko, V. T. 1971, *Soviet Ast.*, 15, 358
- Fernández, R., Monteiro, H., & Schwarz, H. E. 2004, *ApJ*, 603, 595
- Ferrière, K. M. 2001, *Rev. Mod. Phys.*, 73, 1031
- Fich, M., Treffers, R. R., & Dahl, G. P. 1990, *AJ*, 99, 622
- Gaustad, J. E., McCullough, P. R., Rosing, W., & Van Buren, D. 2001, *The Publications of the Astronomical Society of the Pacific (PASP)*, 113, 1326
- Guerrero, M. A., Villaver, E., & Machado, A. 1998, *AJ*, 507, 889
- Haffner, L. M., Reynolds, R. J., & Tufte, S. L. 1998, *ApJ*, 501, L83
- Haffner, L. M., Reynolds, R. J., & Tufte, S. L. 1999, *ApJ*, 523, 223
- Haffner, L. M., Reynolds, R. J., Tufte, S. L., Madsen, G. J., Jaehnig, K. P., & Percival, J. W. 2003, *ApJS*, 149, 405
- Harris, H. C., Dahn, C. C., Monet, D. G., & Pier, J. R. 1997, in *IAU Symp.180, Planetary Nebulae*, ed. H. Habing (Dordrecht: Reidel), 40
- Hoyle, F., & Ellis, G. R. A. 1963, *Australian Journal of Physics*, 16, 1
- Humphreys, R. M. 1978, *ApJS*, 38, 309
- Ishida, K., & Kawajiri, N. 1968, *PASJ*, 20, 95
- Martin, A. G., Elizabeth, G. J., & Chu, Y. H. 2004, *ApJ*, 128, 1705
- Meatheringham, S. J., Wood, P. R., & Faulkner, D. J. 1988, *ApJ*, 334, 862
- Mierkiewicz, E. J. 2002, PhD Thesis, University Of Wisconsin, Madison
- Mierkiewicz, E. J., Roesler, F. L., Nossal, S. M., & Reynolds, R. J. 2006, *Journal of Atmospheric and Solar-Terrestrial Physics (JASTP)*, 68, 1520
- Miller, E. E., & Roesler, F. L. 1998, *Applied Optics*, Department of Physics, University of Wisconsin
- Morgenthaler, J. P., Harris, W. M., & Scherb, F., et al. 2001, *ApJ*, 563, 1, 451
- Muthu, C., & Anandarao, B. G. 2001, *AJ*, 121, 2106
- Nossal, S., Roesler, F. L., Reynolds R. J., & Scherb, F. 1993, *Journal of Geophysical Research*, 98, 3669
- Nossal, S. M. 1994, PhD Thesis, University Of Wisconsin, Madison
- Nossal, S. M., Roesler, F. L., Coakley, M. M., & Reynolds, R. J. 1997, *J. Geophys. Res.*, 102, 14541
- Nossal, S. M., Roesler, F. L., & Coakley, M. M. 1998, *J. Geophys. Res.*, 103, A1, 381
- Nossal, S. M., Roesler, F. L., Reynolds, R. J., et al. 2001, *J. Geophys. Res.*, 106, 5605
- Nossal, S. M., Roesler, F. L., Mierkiewicz, E. J., & Reynolds, R. J. 2004, *Geophys. Res. Lett.*, 31, L06110
- Nossal, S. M., Mierkiewicz, E. J., Roesler, F. L., Reynolds, R. J., & Haffner, L. M. 2006, *Journal of Atmospheric and Solar-Terrestrial Physics (JASTP)*, 68 1553
- Reynolds, R. J., Roesler, F. L., & Scherb, F. 1973, *ApJ*, 179, 651
- Reynolds, R. J., Roesler, F. L., & Scherb, F. 1974, *ApJ*, 192, L53
- Reynolds, R. J. 1988, *ApJ*, 333, 341
- Reynolds, R. J., Roesler, F. L., Scherb, F., & Harlander, J. 1990, in *Instrumentation In Astronomy VII*, ed. D. Crawford (Bellingham: SPIE), 610
- Reynolds, R. J. 1991, *IAU. Printed in the Netherlands*, 67
- Reynolds, R. J., Tufte, S. L., Haffner, L. M., Jaehnig, K., & Percival, J. W. 1998, *Publ. Astron. soc. Aust.*, 15, 14
- Reynolds, R. J. 2004, *Advances in Space Research*, 34, 27
- Reynolds, R. J., Chaudhary, V., Madsen, G. J., & Haffner, L. M. 2005, *AJ*, 129, 927
- Roesler, F. L. 1974, *Methods of Experimental Physics*, Academic Press. Inc. Part 12
- Şahan, M., Yeğingil İ., Kızıloğlu Ü., et al. 2005, *ChJAA (Chin. J. Astron. Astrophys.)*, 5, 211
- Şahan, M., Aksaker N., Yeğingil İ. 2007, *Terrestrial, Atmospheric And Oceanic Sciences (TAO)*, 2007, 18, 1
- Scherb, F. 1981, *ApJ*, 243, 644
- Schneider, S. E., & Terzian Y., 1983, *ApJS*, 52, 399
- Shih, P., Roesler, F. L., & Scherb, F. 1985, *J. Geophys. Res.*, 90, A1, 477
- Treffers, R. R. 1981, *ApJ*, 250, 213
- Tufte, S. L. 1997, PhD. Thesis, University Of Wisconsin, Madison